crystals

MDPI

Article

Phase Compositions and Microwave Dielectric Properties of $Na_{1+x}SrB_5O_{9+0.5x}$ Ceramics

Xuepeng Lu [1], Peng Wu [2,*], Huimin Yang [3], Min Yang [3] and Yong Zheng [3,*]

[1] School of Materials Science and Engineering, Nanjing Institute of Technology, Nanjing 211167, China; xuepenglyu@njit.edu.cn
[2] College of Chemistry and Materials, Longyan University, Longyan 364012, China
[3] College of Materials Science and Technology, Nanjing University of Aeronautics and Astronautics, Nanjing 210016, China
* Correspondence: wupeng@lyun.edu.cn (P.W.); zy_msc@nuaa.edu.cn (Y.Z.)

Abstract: Microwave dielectric ceramics composed of $Na_{1+x}SrB_5O_{9+0.5x}$ ($0 \leq x \leq 0.125$) were synthesized via a traditional solid-state reaction approach. The effects of non-stoichiometric Na on the crystal structures, phase compositions, chemical bond characteristics, and microwave dielectric properties of the $Na_{1+x}SrB_5O_{9+0.5x}$ ceramics were systematically studied. All $Na_{1+x}SrB_5O_{9+0.5x}$ ceramics sintered at optimum temperatures consisted of a $NaSrB_5O_9$ solid-solution phase and a SrB_2O_4 phase. Appropriate excess Na could suppress the generation of the SrB_2O_4 phase, and the lowest content of the SrB_2O_4 phase was achieved at x = 0.075. The ε_r values of the $Na_{1+x}SrB_5O_{9+0.5x}$ ceramics were primarily affected by the relative density and molecular polarization. The $Q \times f$ values showed a positive correlation with the lattice energy. The τ_f value was correlated to the SrB_2O_4 phase content, bond valence, and bond energy. Typically, the $Na_{1.075}SrB_5O_{9.0375}$ ceramic sintered at 825 °C possessed good microwave dielectric properties of ε_r = 5.61, $Q \times f$ = 31, 937 GHz, and τ_f = −3.09 ppm/°C, which are suitable for high-frequency, low-temperature co-fired ceramics (LTCCs) substrate applications.

Keywords: LTCC; borate ceramic; microwave dielectric properties; non-stoichiometric; phase composition

check for updates

Citation: Lu, X.; Wu, P.; Yang, H.; Yang, M.; Zheng, Y. Phase Compositions and Microwave Dielectric Properties of $Na_{1+x}SrB_5O_{9+0.5x}$ Ceramics. *Crystals* **2023**, *13*, 1042. https://doi.org/10.3390/cryst13071042

Academic Editors: Kaixin Song and Maria Gazda

Received: 20 May 2023
Revised: 21 June 2023
Accepted: 27 June 2023
Published: 30 June 2023

Copyright: © 2023 by the authors. Licensee MDPI, Basel, Switzerland. This article is an open access article distributed under the terms and conditions of the Creative Commons Attribution (CC BY) license (https://creativecommons.org/licenses/by/4.0/).

1. Introduction

In recent years, significant advancements have been made in the development of millimeter-wave wireless communications. In order to facilitate the effective utilization of 5G communication, it is imperative to develop innovative microwave dielectric materials that can facilitate the miniaturization and integration of passive electronic components [1–3]. Low-temperature co-fired ceramic (LTCC) technologies play a critical role in enabling the miniaturization and integration of communication equipment [4–6]. To satisfy the demands of low-temperature co-fired ceramic (LTCC) technologies, microwave dielectric ceramics must be sintered at temperatures below 961 °C. Additionally, low permittivity (ε_r) values contribute to improved signal transmission speeds and reduced latencies, while high quality factor ($Q \times f$) values mitigate losses and broaden the bandwidth. Finally, near-zero temperature coefficients of resonance frequency (τ_f) values ensure system stability.

The development of low-temperature synthetic microwave dielectric ceramics has predominantly centered around molybdates, phosphates, vanadates, borates, and glass–ceramics [7–11]. Of these, borate ceramics have received substantial attention in recent years owing to their low raw prices, variable chemical structures, excellent dielectric properties, and straightforward preparation processes. Liu et al. [12] reported that $LiMBO_3$ (M = Ca, Sr) ceramics could be densified at 800 °C with excellent dielectric properties (ε_r = 8.7, $Q \times f$ = 75,000 GHz, and τ_f = −150 ppm/°C and ε_r = 8.6, $Q \times f$ = 60,000 GHz, and τ_f = −39 ppm/°C) and could be chemically compatible with Ag. Zhou et al. [13] prepared dense $Li_6B_4O_9$ microwave dielectric ceramics at 640 °C with microwave dielectric

properties of ε_r = 5.95, Q × f = 41,800 GHz, and τ_f = −72 ppm/°C, and a prototype patch antenna was fabricated by exploiting the compatibility of $Li_6B_4O_9$ with silver metallization using LTCC technology.

$NaSrB_5O_9$, a commonly studied borate due to its complex structural chemistry, has been utilized investigations of its photoluminescence properties [14–16]. Wu et al. [17] first reported the crystal structure of the $NaSrB_5O_9$ compound. The fundamental structural unit in $NaSrB_5O_9$ is the $[B_5O_9]^{3-}$ anionic group, which is constructed from three $[BO_3]$ triangles and two $[BO_4]$ tetrahedra. The Na and Sr atoms are encircled by eight O atoms and form trigonal dodecahedra. In our previous work, we reported that $NaSrB_5O_9$-based ceramics densified at 800 °C exhibited remarkable microwave dielectric properties of ε_r = 5.67, Q × f = 49,824 GHz, and τ_f = −18.28 ppm/°C [18]. Thus, the second phase of SrB_2O_4 was formed in all ceramics sintered at various temperatures and could potentially be attributed to the evaporation of Na and B. Yang et al. [19] found that an excess of B can suppress the formation of the second phase of SrB_2O_4, resulting in improvements in the uniform microstructures of $NaSrB_{5+5x}O_{9+7.5x}$ ceramics. Similarly, Na elements are prone to volatility during the sintering process. However, research on the non-stoichiometric effects of Na on the phase composition and properties of $NaSrB_5O_9$-based ceramics has not been reported yet.

In this study, the sintering behaviors, phase compositions, microstructures, and microwave dielectric properties of $Na_{1+x}SrB_5O_{9+0.5x}$ ($0 \leq x \leq 0.125$) ceramics fabricated via the solid-phase sintering method were thoroughly researched. The intrinsic mechanism responsible for the microwave dielectric properties was elucidated by utilizing the P-V-L bond theory.

2. Experimental Procedure

The analytical reagents, Na_2CO_3 (99.5%), $SrCO_3$ (99%), and H_3BO_3 (≥99.5%), were utilized in the traditional solid-state reaction method to fabricate $Na_{1+x}SrB_5O_{9+0.5x}$ ($0 \leq x \leq 0.125$) ceramics. The powders were weighed according to the aforementioned chemical formulae and mixed with ZrO_2 balls in a nylon jar for 4 h, using ethanol as the mixing medium. The resulting slurries were dried at 80 °C and pre-synthesized at 600 °C for 4 h to obtain the primary phase. The pre-synthesized powders were then re-milled for another 4 h and re-dried. The mixed powders were pressed into cylindrical samples with diameters of 10 mm and thicknesses of 6 mm, using a pressure of 150 MPa. A binder solution containing 5 wt.% of polyvinyl alcohol (PVA) was employed. The green samples were subsequently sintered at temperatures ranging from 750 °C to 850 °C for 4 h.

The phase compositions were analyzed via a powder X-ray diffractometer (Advanced D8, Bruker, Ettlingen, Germany) with CuKα radiation. GSAS and EXPGUI software were utilized to refine the diffraction data to ensure accuracy in determining the crystal structures. The total lattice energy, bond valence, and bond energy were calculated via the P-V-L bond theory [20]. In the case of binary crystals (A_mB_n), the lattice energy (U_{total}) of the ceramic was calculated as follows:

$$U_{total} = \sum U^{\mu} \tag{1}$$

$$U^{\mu} = U_c^{\mu} + U_i^{\mu} \tag{2}$$

$$U_c^{\mu} = 2100 \cdot m \cdot \frac{\left(Z_+^{\mu}\right)^{1.64}}{\left(d^{\mu}\right)^{0.75}} \cdot f_c^{\mu} \tag{3}$$

$$U_i^{\mu} = 1270 \cdot \frac{(m+n) \cdot Z_+^{\mu} \cdot Z_-^{\mu}}{d^{\mu}} \cdot \left(1 - \frac{0.4}{d^{\mu}}\right) \cdot f_i^{\mu} \tag{4}$$

where U_c^{μ} and U_i^{μ} represent the covalent and ionic lattice energies of the μ bond, respectively, and Z_+^{μ} and Z_-^{μ} are the valence states of the cations and anions that constitute the μ bonds, respectively.

The bond energy (E_T) of the ceramic can be obtained as follows:

$$E_T = \sum E_b^\mu \tag{5}$$

$$E_b^\mu = t_c E_c^\mu + t_i E_i^\mu \tag{6}$$

$$E_c^\mu = \frac{(r_{CA} + r_{CB})}{d^\mu} \cdot (E_{A-A} E_{B-B})^{1/2} \tag{7}$$

$$E_i^\mu = \frac{1389.088}{d^\mu} \tag{8}$$

where E_c^μ and E_i^μ represent the covalent and ionic parts of the bond energy, respectively, t_c and t_i represent the scale factors of the covalent and ionic parts, r_{CA} and r_{CB} are the covalent radii of the chemical bonds in A and B, respectively, and E_{A-A} and E_{B-B} are the homonuclear bond energies.

The bond valence (V) of the ceramic is calculated as follows:

$$V = \sum_j V_{ij}/n \tag{9}$$

$$V_{ij} = \exp\left(\frac{R_{ij} - d_{ij}}{b_0}\right) \tag{10}$$

where V_{ij} is the bond valence of each bond, n is the number of bonds, R_{ij} is the bond valence parameter (a fixed value), d_{ij} is the bond length, and b_0 is a constant.

The microstructures of the samples were examined using scanning electron microscopy (SEM; S-3400 N. Hitachi, Tokyo, Japan). The Archimedes method was employed to determine the bulk densities of the ceramic samples. The microwave dielectric properties of the samples were evaluated using the Hakki–Coleman method [21] with a vector network analyzer (Agilent, N5244A, Santa Clara, CA, USA). Five specimens for each ceramic composition were tested, and the arithmetic means of the test results were taken. The resonance frequencies of the samples were measured at both 25 °C and 85 °C to estimate the temperature coefficients of the resonant frequencies (τ_f), which were determined as follows:

$$\tau_f = \frac{f_{85} - f_{25}}{(85 - 25)} \times 10^6 \text{ (ppm/°C)} \tag{11}$$

where f_{25} and f_{85} were the TE01δ resonant frequencies at 25 °C and 85 °C, respectively.

3. Results and Discussion

The trend in the relative densities of the $Na_{1+x}SrB_5O_{9+0.5x}$ microwave dielectric ceramics at different sintering temperatures is illustrated in Figure 1. The relative densities of ceramics with the same compositions initially increases and then decreases with an increase in the sintering temperature. When $0 \leq x \leq 0.05$, the optimum sintering temperature for the $Na_{1+x}SrB_5O_{9+0.5x}$ ceramics is 800 °C. When $x \geq 0.075$, the optimum densification sintering temperature for the $Na_{1+x}SrB_5O_{9+0.5x}$ ceramics increased from 800 °C to 825 °C, indicating that an excessive amount of Na can increase the optimum sintering temperature for the $Na_{1+x}SrB_5O_{9+0.5x}$ ceramics. In addition, a suitable amount of Na can enhance the relative densities of the ceramics sintered at the optimum sintering temperature. Remarkably, the $Na_{1.1}SrB_5O_{9.05}$ ceramic sintered at 825 °C has the maximum relative density of 98.9%, which is higher than the maximum relative density of the $NaSrB_5O_9$ ceramic.

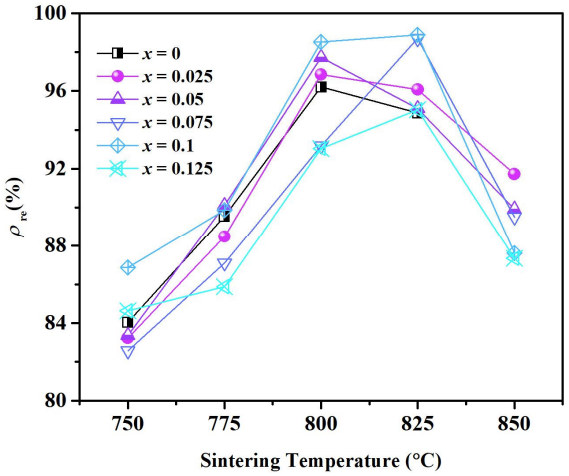


Figure 1. Relative densities of the $Na_{1+x}SrB_5O_{9+0.5x}$ ($0 \leq x \leq 0.125$) ceramics sintered at various temperatures.

Figure 2a displays the XRD patterns of the $Na_{1+x}SrB_5O_{9+0.5x}$ ($0 \leq x \leq 0.125$) ceramics at the optimum sintering temperature. The diffraction peaks of all the samples match well with the standard cards for $NaSrB_5O_9$ (ICDD-PDF 00-056-0415, monoclinic, space group $P2_1/c$) and SrB_2O_4 (ICDD-PDF 00-015-0779, orthorhombic, space group Pbcn). In addition, the diffraction peak intensity of the second phase, SrB_2O_4, in all ceramics is relatively low, which implies that an excessive amount of Na can reduce the formation of the second phase, SrB_2O_4, to a certain extent.

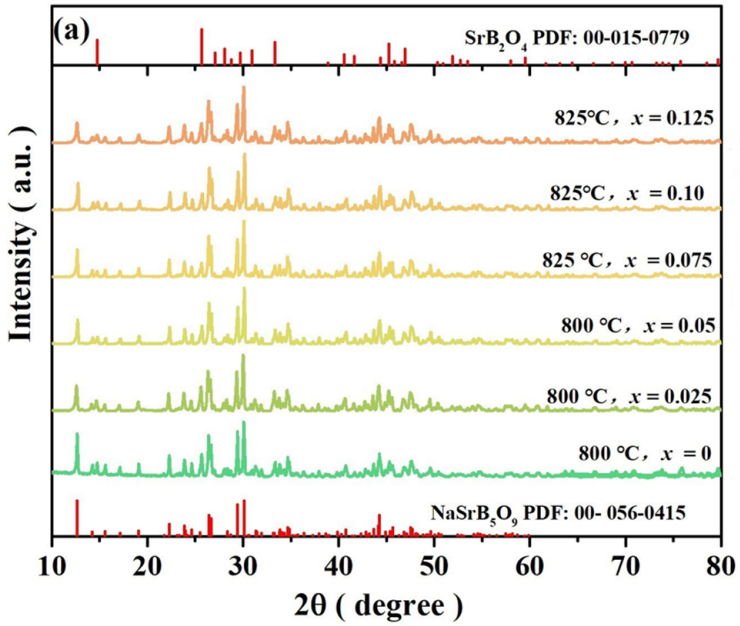


Figure 2. *Cont.*

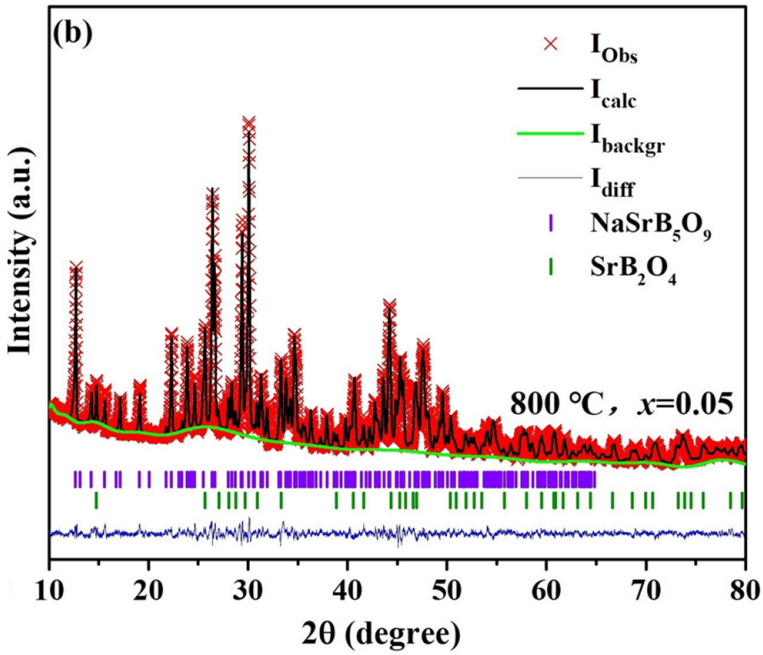


Figure 2. (**a**) The X-ray data of the $Na_{1+x}SrB_5O_{9+0.5x}$ ($0 \leq x \leq 0.125$) ceramics sintered at various temperatures; (**b**) Rietveld refinement pattern for the XRD data (x = 0.05 is taken as an example).

Crystal structure refinements were performed on powder samples using GSAS software. The calculated patterns of all samples closely fit those of measured, indicating that the refinement results are credible. The pattern following the refinement of the $Na_{1+x}SrB_5O_{9+0.5x}$ (x = 0.05) ceramics sintered at 800 °C is shown in Figure 2b. The lattice parameters and phase composition fractions are listed in Table 1. When $0 \leq x \leq 0.1$, the unit cell volume of the $NaSrB_5O_9$ phase increases with an increase in x, probably due to the partial entry of Na+ ions into the interstitial sites, resulting in an enlargement of the unit cell volume of the $NaSrB_5O_9$ phase. When x continues to increase, the unit cell volume slightly decreases. It is noted that excessive Na can suppress the formation of the second phase, SrB_2O_4, and the minimum mass percentage of the SrB_2O_4 phase (content: 9.05 wt.%) was obtained at x = 0.075.

Table 1. Lattice and refinement data of $Na_{1+x}SrB_5O_{9+0.5x}$ ($0 \leq x \leq 0.125$) ceramics sintered at optimum temperatures.

x	Phase	*a* (Å)	b (Å)	*c* (Å)	*V* (Å^3)	*wt. %*	R_{wp}	R_p	χ^2
0	$NaSrB_5O_9$	6.4755	13.9231	8.0265	692.412	81.38	5.86%	4.36%	2.78
	SrB_2O_4	11.9770	4.3231	6.5811	340.714	18.62			
0.025	$NaSrB_5O_9$	6.4957	13.9698	8.0489	698.873	82.81	1.93%	1.45%	2.808
	SrB_2O_4	12.0605	4.3581	6.6351	348.752	17.19			
0.050	$NaSrB_5O_9$	6.5024	13.9818	8.0543	700.614	85.04	2.36%	1.85%	3.274
	SrB_2O_4	12.0267	4.3422	6.6080	345.084	14.96			
0.075	$NaSrB_5O_9$	6.5030	13.9840	8.0561	700.976	90.95	1.88%	1.44%	2.845
	SrB_2O_4	12.0359	4.3450	6.6138	345.873	9.05			
0.100	$NaSrB_5O_9$	6.5058	13.9907	8.0601	701.979	88.77	1.89%	1.34%	2.972
	SrB_2O_4	12.0488	4.3518	6.6235	347.299	11.23			
0.125	$NaSrB_5O_9$	6.5009	13.9824	8.0537	701.465	87.16	2.24	1.56	3.276
	SrB_2O_4	12.0244	4.3448	6.6099	345.323	12.84			

R_p—the reliability factor of patterns. R_{wp}—the reliability factor of weighted patterns. χ^2—the goodness of fit indicator = chi.2.

Figure 3 shows the microstructures of the $Na_{1+x}SrB_5O_{9+0.5x}$ ($0 \leq x \leq 0.125$) ceramics sintered at optimum temperatures. It can be seen that the grains of all samples are tightly

arranged with each other, but irregular polygonal grains appear with the increase in the Na content. When $x \geq 0.05$, the grain size increases, the grain boundaries become blurred, and the morphologies of the grains change in the samples. The number of nearly equiaxed grains decreases significantly, while the number of polygonal grains increases, and there are also abnormally large grains in Figure 3f.

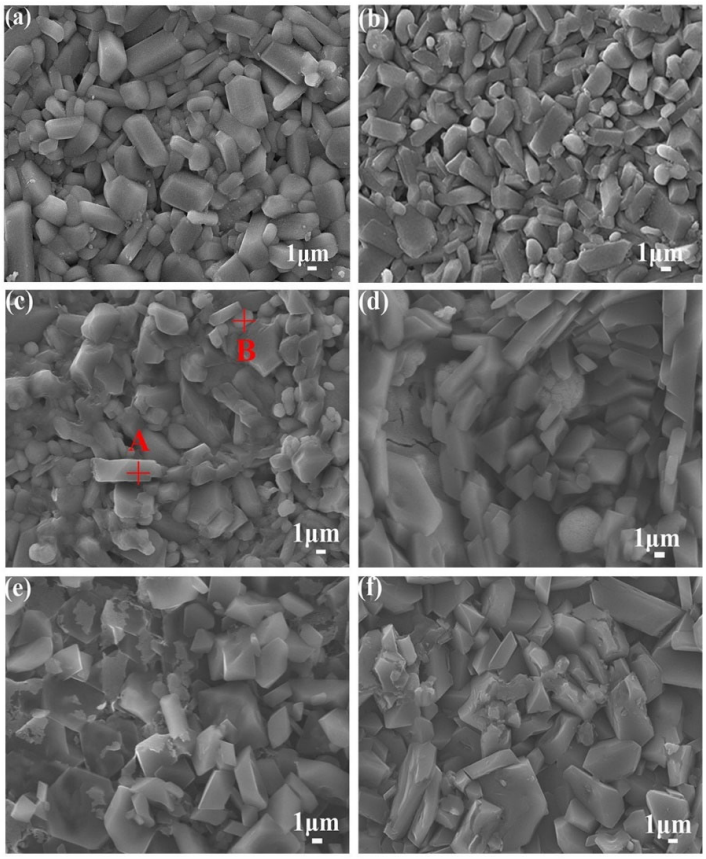


Figure 3. SEM micrographs of the $Na_{1+x}SrB_5O_{9+0.5x}$ ($0 \leq x \leq 0.125$) ceramics sintered at optimum temperatures: (**a**) x = 0, 800 °C; (**b**) x = 0.025, 800 °C; (**c**) x = 0.050, 800 °C; (**d**) x = 0.075, 825 °C; (**e**) x = 0.100, 825 °C; (**f**) x = 0.125, 825 °C.

In order to analyze the elemental compositions of the polygonal grains in the ceramic samples, EDS testing was conducted on the labeled grains in Figure 3c, and the results are shown in Figure 4. The EDS elemental analysis results indicate that the elements contained in the two types of grains (A and B) are the same, including Na, Sr, B, and O, and their atomic ratios are similar, indicating that they belong to the same solid-solution phase.

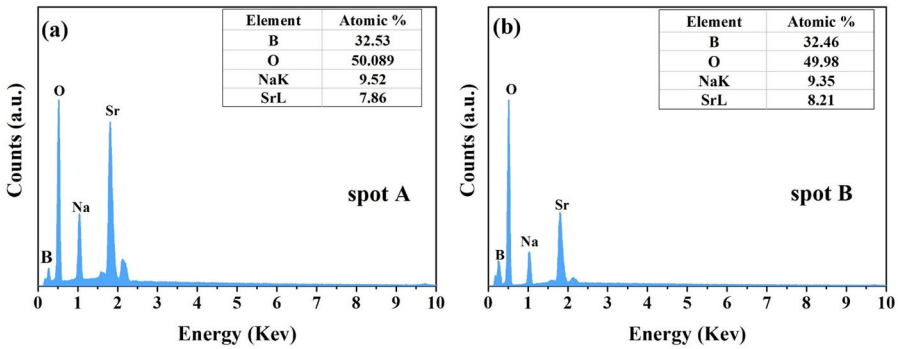


Figure 4. EDS spectra of the grains in $Na_{1+x}SrB_5O_{9+0.5x}$ (x = 0.05) ceramics: (**a**) spot A; (**b**) spot B.

The ε_r values of the $Na_{1+x}SrB_5O_{9+0.5x}$ ceramics at different sintering temperatures are shown in Figure 5a. The ε_r values of all compositions increase first and then decrease with the increase in sintering temperature, which agrees well with the variation trend of the relative densities of the ceramics, indicating that the relative density is the main factor for ε_r values.

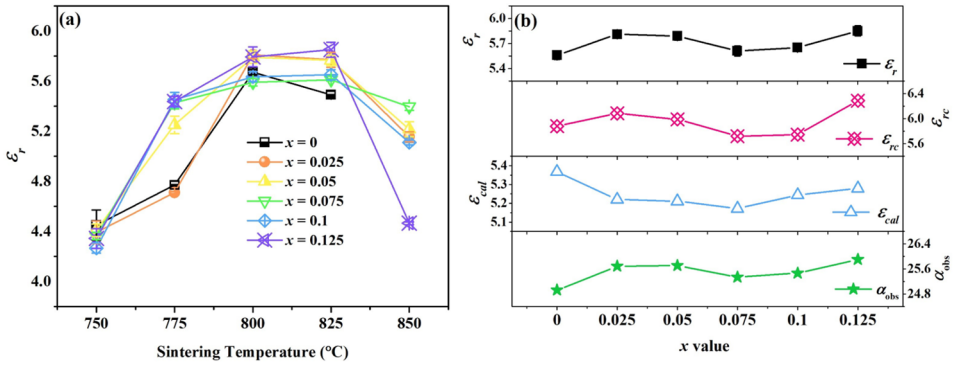


Figure 5. (**a**) ε_r values of $Na_{1+x}SrB_5O_{9+0.5x}$ ceramics sintered at different temperatures; (**b**) ε_r, ε_{rc}, ε_{cal}, and α_{obs} values of $Na_{1+x}SrB_5O_{9+0.5x}$ ceramics sintered at optimum temperatures.

To further discuss the influence of the Na content on the ε_r values of $Na_{1+x}SrB_5O_{9+0.5x}$ ceramics sintered at optimum temperatures, the corrected dielectric constant (ε_{rc}) was obtained by correcting the measured dielectric constant (ε_r) of the ceramics for porosity, and the theoretical dielectric constant (ε_{cal}) and the actual molecular polarization (α_{obs}) were calculated based on the refined results, as shown in Figure 5b. The values were determined as follows [22–24]:

$$\varepsilon_{rc} = \varepsilon_r(1 + 1.5P) \tag{12}$$

$$\varepsilon_{cal} = \frac{3V_m + 8\pi\alpha_{theo}}{3V_m - 4\pi\alpha_{theo}} \tag{13}$$

$$\begin{aligned}\alpha_{theo}(Na_{1+x}SrB_5O_{9+0.5x}) = (1+x) \times \alpha\left(Na^{+}\right) + \alpha\left(Sr^{2+}\right) \\ +5\alpha\left(B^{3+}\right) + (9+0.5x) \times \alpha\left(O^{2-}\right)\end{aligned} \tag{14}$$

$$\alpha_{theo}(SrB_2O_4) = \alpha\left(Sr^{2+}\right) + 2\alpha\left(B^{3+}\right) + 4\alpha\left(O^{2-}\right) \tag{15}$$

$$\ln \varepsilon_{cal} = \sum_i^n V_i \ln \varepsilon_i \tag{16}$$

where P is fractional porosity, V_m is the molecular volume, α_{theo} is the theoretical polarizability, and V_i represents the volume fraction of each phase: $\alpha(Na^+)$ = 1.8 Å^3, $\alpha(Sr^{2+})$ = 4.24 Å^3, $\alpha(B^{3+})$ = 0.05 Å^3, and $\alpha(O^2)$ = 2.01 Å^3 [25].

The Clausius–Mosotti equation can be utilized to determine the observed ionic polarizability, which is calculated as follows [26]:

$$\alpha_{obs} = \frac{3V(\varepsilon_r - 1)}{4\pi(\varepsilon_r + 2)} \tag{17}$$

where V is the volume of the unit cell.

The trend in the variation of ε_r values is consistent with those of ε_{rc} and α_{obs} but inconsistent with that of ε_{cal}, indicating that relative density and molecular polarization are important factors influencing the ε_r values of $Na_{1+x}SrB_5O_{9+0.5x}$ ceramics.

Figure 6 shows the Q × f values of $Na_{1+x}SrB_5O_{9+0.5x}$ ceramics sintered at different temperatures. It can be seen that the Q × f values of $Na_{1+x}SrB_5O_{9+0.5x}$ ceramics with the same composition first increase and then decrease with an increasing sintering temperature due to reductions in the extrinsic losses caused by decreases in pore and grain boundary

defects. The maximum Q × f value is obtained at the optimal sintering temperature, after which the Q × f value decreases as the grain grows abnormally large. In addition, among all the compositions with excess Na, $Na_{1+x}SrB_5O_{9+0.5x}$ (x = 0.05, Ts = 800 °C) shows the highest Q × f value of 38,453 GHz, indicating that excess Na will deteriorate the dielectric properties of ceramics.

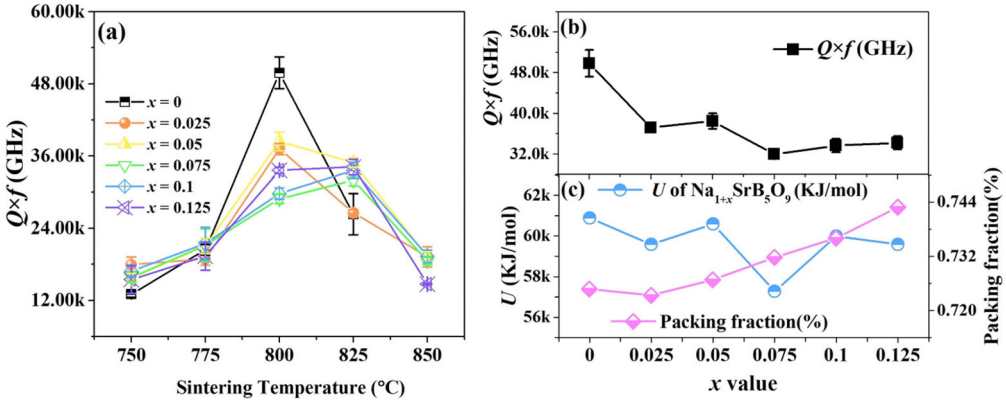


Figure 6. (**a**) Q × f values of $Na_{1+x}SrB_5O_{9+0.5x}$ ceramics sintered at different temperatures; (**b**) Q × f, U and packing fraction values of $Na_{1+x}SrB_5O_{9+0.5x}$ ceramics sintered at optimum temperatures.

In To further understand the variation in the Q × f values of $Na_{1+x}SrB_5O_{9+0.5x}$ ceramics, the total lattice energies (U) and atomic packing densities of $Na_{1+x}SrB_5O_{9+0.5x}$ ceramics were calculated. The atomic packing density is calculated as follows [27]:

$$\begin{aligned} Atom\ packing\ fraction &= \frac{Volume\ of\ the\ atoms\ in\ the\ cell}{Volume\ of\ unit\ cell} \times Z \\ &= \frac{4\pi}{3} \times 4 \times \frac{(1+x)\times r_{Na}^3 + r_{Sr}^3 + 5r_B^3 + (9+0.5x)\times r_O^3}{abc} \end{aligned} \quad (18)$$

where Z is the molecular number in a unit cell.

Typically, a higher lattice energy and atomic packing density lead to a reduction in the intrinsic loss and an enhanced quality factor of a ceramic material. As shown in Figure 6b, the variation trend of the Q × f values showed a positive correlation with U values and an inverse correlation with atomic packing density, implying that the lattice energy has a major impact on the Q × f value of a $Na_{1+x}SrB_5O_{9+0.5x}$ ceramic. The larger lattice energy corresponds to a more stable crystal structure with a minimum intrinsic loss due to non-harmonic lattice vibration.

The τ_f values of microwave dielectric ceramics are influenced by their phase compositions, bond energies, and bond valences. Generally, a higher bond valence (V) and bond energy (E) correspond greater strengths of the chemical bonds and a smaller $|\tau_f|$ value. Figure 7 depicts the τ_f values, bond valences, and bond energies of $Na_{1+x}SrB_5O_{9+0.5x}$ ceramics sintered at optimum temperatures. When $x \leq 0.05$, the τ_f values slightly increase, which is mainly related to the reduction in the second phase, SrB_2O_4, content. When x = 0.075, the ceramic sintered at 825 °C exhibits the maximum τ_f value of −3.09 ppm/°C, which is correlated to the lower second phase content and increases in the bond valence and bond energy. However, as the x value further increases, the τ_f values decrease due to the increase in the second phase content.

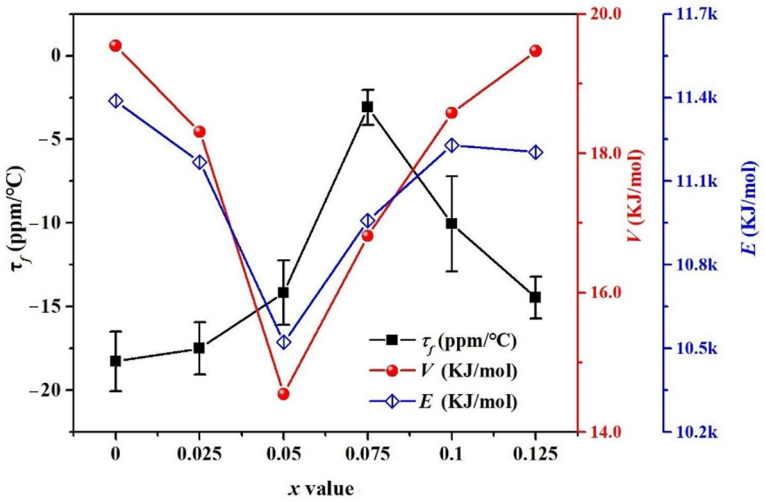


Figure 7. Variations in the τ_f values, bond valences, and bond energies of $Na_{1+x}SrB_5O_{9+0.5x}$ ceramics sintered at optimum temperatures.

Table 2 lists the sintering temperatures and microwave dielectric properties of several borate ceramics. Generally, borate ceramics exhibit low sintering temperatures, low permittivity values, and high Q × f values, rendering them proficient for utilization in low-temperature co-fired ceramics. Compared to the $CaAlB_2O_{5.5}$ and $Zn_3B_2O_6$ systems, the $NaSrB_5O_9$ system exhibits a lower sintering temperature and a τ_f value closer to zero. In comparison to the $LiBO_2$ system, the $NaSrB_5O_9$ system has a higher Q × f value and a τ_f value that is closer to zero. Furthermore, the $Na_{1.075}SrB_5O_{9.0375}$ ceramic has a τ_f value that is closer to zero than the $NaSrB_5O_9$ ceramic. In this work, the $Na_{1.075}SrB_5O_{9.0375}$ ceramic exhibited a low densification temperature (825 °C), a near-zero τ_f value (−3.09 ppm/°C), a high Q × f value (31,937 GHz), and a low dielectric constant (5.61), making it suitable for LTCC applications.

Table 2. The sintering temperatures and microwave dielectric properties of some borate ceramics.

Compounds	S. T. (°C)	ε_r	Q × f (GHz)	τ_f (ppm/°C)	Ref.
$CaAlB_2O_{5.5}$	940	5.8	63,338	−29	[28]
$Zn_3B_2O_6$	925	6.7	58,500	−58	[29]
$(Zn_{0.95}Ni_{0.05})_3B_2O_6$	900	6.9	91,000	−55.6	[30]
$LiBO_2$	640	5.3	18,200	−66.2	[31]
$NaSrB_5O_9$	850	5.67	49,824	−18.28	[17]
$NaSrB_{5.35}O_{9.525}$	825	5.68	57,173	−14.83	[18]
$Na_{1.075}SrB_5O_{9.0375}$	825	5.61	31,937	−3.09	This work

4. Conclusions

Microwave dielectric ceramics composed of $Na_{1+x}SrB_5O_{9+0.5x}$ ($0 \leq x \leq 0.125$) were synthesized via a traditional solid-state reaction approach. The samples sintered at optimum temperatures contained a $Na_{1+x}SrB_5O_{9+0.5x}$ solid-solution phase and SrB_2O_4 phase. Excessive Na can suppress the formation of the second phase, SrB_2O_4, and the minimum mass percentage of the SrB_2O_4 phase (content: 9.05 wt.%) was obtained at x = 0.075. The ε_r values of the $Na_{1+x}SrB_5O_{9+0.5x}$ ceramics were mainly related to the relative density and molecular polarization. The Q × f values showed a positive correlation with lattice energy. The τ_f value was dependent on the second phase content, bond valence, and bond energy. Temperature-stable microwave dielectric ceramics composed of $Na_{1.075}SrB_5O_{9.0375}$ were obtained at 825 °C and exhibited good microwave dielectric properties of ε_r = 5.61, Q × f = 31,937 GHz, and τ_f = −3.09 ppm/°C, which are suitable for high-frequency LTCC substrate applications.

Author Contributions: Writing—original draft preparation, X.L.; methodology, X.L. and H.Y.; software, H.Y.; investigation, H.Y. and M.Y.; data curation, X.L. and P.W.; characterization, P.W.; supervision, Y.Z. All authors have read and agreed to the published version of the manuscript.

Funding: This work was funded by the National Natural Science Foundation of China (NO. 51602145), the Natural Science Foundation of Jiangsu Educational Commission (NO. 22KJB430025), and the Natural Science Foundation of Fujian Province (NO. 2022J011151).

Institutional Review Board Statement: Not applicable.

Informed Consent Statement: Not applicable.

Data Availability Statement: Data is unavailable due to privacy.

Acknowledgments: This work was funded by the National Natural Science Foundation of China (NO. 51602145), the Natural Science Foundation of Jiangsu Educational Commission (NO. 22KJB430025), and the Natural Science Foundation of Fujian Province (NO. 2022J011151).

Conflicts of Interest: The authors declare no conflict of interest.

References

1. Lou, W.; Mao, M.; Song, K.; Xu, K.; Liu, B.; Li, W.; Yang, B.; Qi, Z.; Zhao, J.; Sun, S.; et al. Low permittivity cordierite-based microwave dielectric ceramics for 5G/6G telecommunications. *J. Eur. Ceram. Soc.* **2022**, *42*, 2820–2826. [CrossRef]
2. Lan, X.; Li, J.; Zou, Z.; Xie, M.; Fan, G.; Lu, W.; Lei, W. Improved sinterability and microwave dielectric properties of $[Zn_{0.5}Ti_{0.5}]^{3+}$-doped $ZnAl_2O_4$ spinel solid solution. *J. Am. Ceram. Soc.* **2019**, *102*, 5952–5957. [CrossRef]
3. Hsu, T.H.; Huang, C.L. Low-loss microwave dielectric of novel $Li_{1-2x}M_xVO_3$ (M = Mg, Zn) (x = 0–0.09) ceramics for ULTCC applications. *J. Eur. Ceram. Soc.* **2021**, *41*, 5918–5923. [CrossRef]
4. Chi, M.; Liu, Y.; Zhao, J.; Dong, C.; Luo, X.; Wang, D.; Liu, B.; Mao, M.; Shi, F.; Song, K. $Mg_3B_2O_6$ microwave dielectric ceramics fabricated by combining cold sintering with post-annealing process. *J. Am. Ceram. Soc.* **2023**, *106*, 285–292. [CrossRef]
5. Yu, H.; Liu, J.; Zhang, W.; Zhang, S. Ultra-low sintering temperature ceramics for LTCC applications: A review. *J. Mater. Sci. Mater. Electron.* **2015**, *26*, 9414–9423. [CrossRef]
6. Liu, W.; Zuo, R. Low temperature fired $Ln_2Zr_3(MoO_4)_9$ (Ln = Sm, Nd) microwave dielectric ceramics. *Ceram. Int.* **2017**, *43*, 17229–17232. [CrossRef]
7. Fang, L.; Su, C.; Zhou, H.; Wei, Z.; Zhang, H.; Alford, N. Novel low-firing microwave dielectric ceramic $LiCa_3MgV_3O_{12}$ with low dielectric loss. *J. Am. Ceram. Soc.* **2013**, *96*, 688–690. [CrossRef]
8. Cho, I.S. Sintering behavior and dielectric properties of $A_3(PO_4)_2$ compounds (A = Ca, Sr, Ba, Mg, Zn, Ni, Cu). *Mat. Sci. Semicon. Proc.* **2022**, *148*, 106793. [CrossRef]
9. Choi, Y.J.; Park, J.H.; Ko, W.J.; Hwang, I.S.; Park, J.H.; Park, J.G.; Nahm, S. Co-firing and shrinkage matching in low- and middle-permittivity dielectric compositions for a low-temperature Co-fired ceramics system. *J. Am. Ceram. Soc.* **2006**, *89*, 562–567. [CrossRef]
10. Yoon, S.H.; Kim, D.W.; Cho, S.Y.; Hong, K.S. Investigation of the relations between structure and microwave dielectric properties of divalent metal tungstate compounds. *J. Eur. Ceram. Soc.* **2006**, *26*, 2051–2054. [CrossRef]
11. Tian, H.; Liu, X.; Yang, Y.; Wu, H.; Zhang, Z. Crystal structure, infrared spectra, and microwave dielectric properties of $Ce_2(Zr_{0.94}Sn_{0.06})_3(MoO_4)_9$ ceramics with low sintering temperature. *Front. Mater.* **2020**, *7*, 145. [CrossRef]
12. Liu, Y.; Wang, Y.; Li, Y.; Bian, J. Low temperature sintering and microwave dielectric properties of $LiMBO_3$ (M = Ca, Sr) ceramics. *Ceram. Int.* **2016**, *42*, 6475–6479.
13. Zhou, D.; Pang, L.; Wang, D.; Qi, Z.; Reaney, I.M. High quality factor, ultralow sintering temperature $Li_6B_4O_9$ microwave dielectric ceramics with ultralow density for antenna substrates. *ACS Sustain. Chem. Eng.* **2018**, *6*, 11138–11143. [CrossRef]
14. Dillip, G.R.; Ramesh, B.; Madhukar Reddy, C.; Mallikarjuna, K.; Ravi, O.; Dhoble, S.J.; Joo, S.W.; Deva Parasad Raju, B. X-ray analysis and optical studies of Dy^{3+} doped $NaSrB_5O_9$ microstructures for white light generation. *J. Alloys Compd.* **2014**, *615*, 719–727. [CrossRef]
15. Raikwar, V.; Bhatkar, V.; Omanwar, S. Morphological and photoluminescence study of $NaSrB_5O_9$: Tb^{3+} nanocrystalline phosphor. *J. Asian Ceram. Soc.* **2018**, *6*, 359–367. [CrossRef]
16. Dillip, G.R.; Mallikarjuna, K.; Dhoble, S.J.; Deva Prasad Raju, B. The luminescence and structural characteristics of Eu^{3+}- doped $NaSrB_5O_9$ phosphor. *J. Phys. Chem. Solid.* **2014**, *75*, 8–14. [CrossRef]
17. Wu, L.; Zhang, Y.; Chen, X.; Kong, Y.; Sun, T.; Xu, J.; Xu, Y. The Na_2O-SrO-B_2O_3 diagram in the B-rich part and the crystal structure of $NaSrB_5O_9$. *J Solid State Chem.* **2007**, *180*, 1470–1475. [CrossRef]
18. Yang, H.; Zheng, Y.; Lu, X.; Xue, C.; Han, Z.; Li, X.; Yang, M. Synthesis of a new sodium strontium borate composite ceramic and its microwave dielectric properties. *Ceram. Int.* **2021**, *47*, 30980–30984. [CrossRef]
19. Yang, M.; Zou, H.; Yang, H.; Zheng, Y.; Xu, X.; Chen, M.; Liang, H.; Zhang, X. Phase composition and microwave dielectric properties of $NaSrB_{5+5x}O_{9+7.5x}$ composite ceramics. *J. Eur. Ceram. Soc.* **2023**, *43*, 1964–1971. [CrossRef]

20. Zhong, M.; Tang, X.; Li, Y.; Jing, Y.; Su, H. Microwave dielectric properties, microstructure, and bond energy of $Zn_{3-x}Co_xB_2O_6$ low temperature fired ceramics. *Ceram. Int.* **2020**, *46*, 18667–18674. [CrossRef]
21. Hakki, B.W.; Coleman, P.D. A dielectric resonant method of measuring inductive capacitance in the millimeter range. *IRE Trans. Microwave Theory Technol.* **1960**, *8*, 402–410. [CrossRef]
22. Bosman, A.J.; Havinga, E.E. Temperature dependence of dielectric constants of cubic ionic compounds. *Phys. Rev.* **1963**, *129*, 1593–1600. [CrossRef]
23. Shannon, R.D.; Rossman, G.R. Dielectric constants of silicate garnets and the oxide additivity rule. *Am. Miner.* **1992**, *77*, 94–100.
24. Zhang, Q.; Tang, X.; Li, Y.; Jing, Y.; Su, H. Influence of substituting Na^+ for Mg^{2+} on the crystal structure and microwave dielectric properties of $Mg_{1-x}Na_{2x}WO_4$ ceramics. *J. Eur. Ceram. Soc.* **2020**, *40*, 4503–4508. [CrossRef]
25. Shannon, R.D. Dielectric polarizabilities of ions in oxides and fluorides. *J. Appl. Phys.* **1993**, *73*, 348–366. [CrossRef]
26. Maex, K.; Baklanov, M.R.; Shamiryan, D.; Lacopi, F.; Brongersma, S.H.; Yanovitskaya, Z.S. Low dielectric constant materials for microelectronics. *J. Appl. Phys.* **2003**, *93*, 8793–8841. [CrossRef]
27. Song, X.; Zou, Z.; Lu, W.; Chen, T.; Ta, S.; Fu, Z.; Lei, W. Crystal structure, lattice energy and microwave dielectric properties of melilite-type $Ba_{1-x}Sr_xCu_2Si_2O_7$ solid solutions. *J. Alloys Compd.* **2020**, *835*, 155340. [CrossRef]
28. Yang, H.; Zhang, S.; Wen, Q.; Yuan, Y.; Li, E. Synthesis of $CaAl_{2x}B_2O_{4+3x}$: Novel microwave dielectric ceramics with low permittivity and low loss. *J. Eur. Ceram. Soc.* **2021**, *41*, 2596–2601. [CrossRef]
29. Wu, X.; Wang, H.; Chen, Y.; Zhou, D. Synthesis and microwave dielectric properties of $Zn_3B_2O_6$ ceramics for substrate application. *J. Am. Ceram. Soc.* **2012**, *95*, 1793–1795. [CrossRef]
30. Peng, R.; Su, H.; Li, Y.; Lu, Y.; Yu, C.; Shi, L.; Chen, D.; Liao, B. Microstructure and microwave dielectric properties of Ni doped zinc borate ceramics for LTCC applications. *J. Alloys Compd.* **2021**, *868*, 159006. [CrossRef]
31. Yin, C.; Du, K.; Zhang, M.; Yang, J.; Wang, F.; Guo, Y.; Cheng, M.; Cai, Y.; Song, X.; Khaliq, J.; et al. Novel low-ε_r and lightweight $LiBO_2$ microwave dielectric ceramics with good chemical compatibility with silver. *J. Eur. Ceram. Soc.* **2022**, *42*, 4580–4586. [CrossRef]

Disclaimer/Publisher's Note: The statements, opinions and data contained in all publications are solely those of the individual author(s) and contributor(s) and not of MDPI and/or the editor(s). MDPI and/or the editor(s) disclaim responsibility for any injury to people or property resulting from any ideas, methods, instructions or products referred to in the content.